A numerical study of crack-tip plasticity in glassy polymers

Lai, J.; van der Giessen, E.

Published in:
Mechanics of Materials

DOI:
10.1016/S0167-6636(97)00006-9

Publication date:
1997

ELSEVIER

Mechanics of Materials 25 (1997) 183–197

MECHANICS OF MATERIALS

A numerical study of crack-tip plasticity in glassy polymers

J. Lai, E. Van der Giessen *

Delft University of Technology, Laboratory for Engineering Mechanics, Mekelweg 2, 2628 CD Delft, The Netherlands

Received 23 July 1996; received in revised form 10 December 1996; accepted 20 January 1997

Abstract

This paper reports on a finite element analysis of the crack-tip plastic zone and near-tip fields in viscoplastic glassy amorphous polymers. The constitutive model employed in this study accounts for the typical shear yielding behavior of glassy polymers, i.e., the intrinsic softening upon yielding and the subsequent orientational strain hardening. The small scale yielding, boundary layer approach is adopted to model the local finite-strain deformation processes in front of a crack with a blunt notch. Numerical results show that the shape of the plastic zone near the tip of a Mode I crack in a glassy polymer depends sensitively on the combined effect of softening and strain hardening. Softening tends to intensify the plastic deformation, while the subsequent hardening tends to depress plastic flow and gives rise to continuous propagation of the current plastic zone. Thus, the plastic zone in typical amorphous polymers is found to be quite different from the HRR solution for yielding in hardening metals. It is also found that the distribution of hydrostatic stress, which is probably responsible for crazing, is intimately related to the pattern of the plastic deformation in front of the crack tip.

PACS: 61.41.+e
Keywords: Polymer; Crack; Plastic zone; Viscoplasticity; Crazing; Shear band; Crack-tip opening displacement

1. Introduction

Although amorphous glassy polymers, like polystyrene (PS), styrene–acrylonitrile (SAN), polymethyl-methacrylate (PMMA) and polycarbonate (PC), usually fail in a rather brittle manner, there is an important class of these materials that may also undergo substantial plastic deformation. In many materials, like in PS, SAN and PMMA, crazing is the dominant fracture mechanism (Kramer, 1983), but not, for instance, in PC. When crazing is suppressed, for instance under compressive loading, materials such as PMMA, SAN and PC can be deformed to large plastic strains of the order of 100% or more by a mechanism that is referred to in the polymer community as 'shear yielding'. But also in tension, these materials may exhibit plastic flow locally near the tip of a crack or near a blunted notch. The subsequent shielding by the plastic zone can strongly influence the fracture resistance. Crazing and plastic shearing are usually thought to be two coupled mechanisms prior to fracture of most glassy polymers. However, recent experiments (Yamamoto and Furukawa, 1995; Ishikawa, 1995) have shown that craze initiation in some polymers does not occur until the crack-tip plastic zone has developed to a critical extent. Therefore, a proper description of the plastic deformation zone near the crack tip is vitally important for the understanding of the fracture mechanisms in these polymers. As a first

* Corresponding author. Tel.: +31-15-2786500; fax: +31-15-2782150; e-mail: e.vandergiessen@wbmt.tudelft.nl.

PII S0167-6636(97)00006-9

step, this paper will focus entirely on the crack tip plastic zone; the competition with fracture mechanisms is not included here.

The role of plastic deformation near crack tips in metals has been studied in great detail in the past, and to various degrees of sophistication. At the most elementary level, the Von Mises and Tresca yield criteria employed to the elastic singular field provide the mutually similar, kidney-shaped plastic zones in front of the tip of a mode I crack. For power-law hardening materials, classical small-strain solutions for near-tip plastic fields under small-scale yielding conditions are due to Hutchinson (1968) and Rice and Rosengren (1968) (HRR fields). Finite-strain effects under mode 1, leading to blunting of the tip, were considered in terms of slip-line fields by Rice and Johnson (1970), and the first full-field numerical solutions were due to McMeeking (1977).

However, the interpretation of crack-tip plastic deformation in polymers is still at a speculative level with regard to a detailed understanding. This is mainly caused by the fact that polymers exhibit quite a different, and in many respects more complicated plastic behavior than metals. It has been well recognized that glassy amorphous polymers exhibit plastic deformation below the glass transition temperature through the activation of microscopic shear bands, giving rise to a macroscopically viscoplastic response. While strain hardening in metals is largest right after yield, plasticity in amorphous polymers is characterized by softening immediately after yield, followed by progressive strain hardening at large deformations (e.g., Bowden, 1973), as illustrated schematically in Fig. 1. This makes amorphous polymers highly prone to localization of deformation in shear bands. When subjected to shearing deformation, as a simple example, a shear band initiates at the onset of yielding at a shear stress τ_y. During further localization, the shear stress drops to some minimum value τ_{min} and while deformation inside the band continues, stress increases again until it reaches a value of τ_y again at γ_b. At that point, neighboring material will yield and exhibit strain localization, so that the shear band propagates through the material, with the material inside the band experiencing a limited shear of γ_b. Under prescribed loading, localization involves substantially enhanced shear rates inside the band, with band propagation taking place at essentially the same band strain γ_b. The well-known phenomena of neck propagation in polymers occurs by a similar process. This particular constitutive behavior is likely to be an important factor influencing the fracture of glassy polymers, whereas so far the classical results for metals cited above are often directly used or transplanted to fracture problems of polymers (e.g., Williams, 1984). Up to now the linkage between the crack-tip plastic deformation and the constitutive behavior of polymers seems to be lacking.

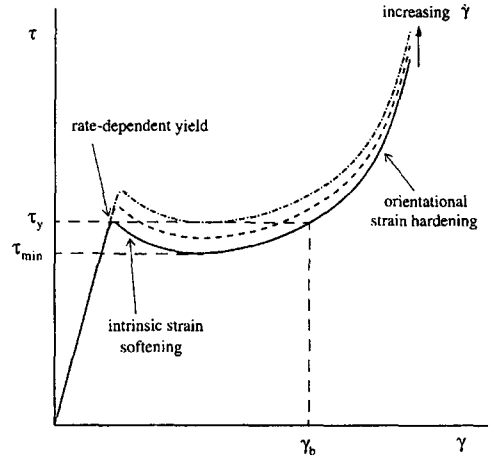

Fig. 1. Schematic of the shear stress versus shear strain response of amorphous glassy polymers.

These matters are further complicated by the experimental difficulty to directly observe the crack-tip plastic zone in polymers at practical crack-tip dimensions. Many studies have been made of the crack tip processes in polymer blends, in which the dispersion of second-phase particles assist to monitor the deformation fields. Light microscopy is then able to reveal a stress whitened zone near the crack tip, with sizes of the order of millimeters. However, such zones are usually a compound consequence of local microvoiding and crazing (Ni et al., 1991), which overlay shear bands in front of the crack tip. Unfortunately, light microscopy cannot be used to study the plastic zones at smaller size scales. Jeong et al. (1994) therefore performed four-point bending experiments using specimens with millimeter wide notches in order to obtain plastic zones at the millimeter range. Thus, they observed plastic deformation in the form of shear bands, often comprising many fine slip lines, in pure epoxy and in rubber-toughened epoxy

specimens. Similar plastic zones were observed in three-point bending specimens made of polycarbonate (PC) blended with poly(acrylonitrile–butadiene–styrene) (ABS) by Ishikawa (1995). In these studies, it was recognized that craze initiation is related to the plastic zone in front of notches. In some glassy amorphous polymers (Yamamoto and Furukawa, 1995) as well as in polymer blends (Ishikawa, 1995), craze initiation was found to occur at the tip of the plastic zone as soon as the plastic zone reached a critical size.

The objective of this paper is to provide some basic understanding of the plastic flow in amorphous glassy polymers near crack tips, by way of a numerical study of the crack-tip plastic zone and near-tip fields under Mode I loading conditions. The local deformation processes around a plane strain Mode I crack are modelled within the framework of small scale yielding using the boundary layer approach. A finite strain formulation is adopted in order to account for the large deformation behavior and crack tip blunting. The rate-dependent material response is described by a recent 3D elastic–viscoplastic constitutive model (Boyce et al., 1988; Wu and Van der Giessen, 1993) that attempts to incorporate the key features of plastic flow in amorphous glassy polymers mentioned above. A parameter study is performed to examine the effects of softening and hardening on the local plastic deformation near the crack tip. The distribution of mean normal stress (hydrostatic stress) and the crack-tip opening displacement are also discussed.

2. Material model

The material model employed in this study is based on the 3D elastic–viscoplastic model for amorphous polymers proposed originally by Boyce et al. (1988) and modified by Wu and Van der Giessen (1993). This model incorporates the initial linear elastic response and the rate-dependent yield of the material, including the intrinsic softening upon yielding, and nonlinear strain hardening at large plastic deformations. We only give a brief recapitulation of the constitutive model here, using the formulation in Wu and Van der Giessen (1993, 1996).

The Eulerian strain rate $\mathbf{D}$ is decomposed into an elastic part $\mathbf{D}^e$ and a plastic part $\mathbf{D}^p$,

$$\mathbf{D} = \mathbf{D}^e + \mathbf{D}^p. \tag{1}$$

Assuming the elastic strains to remain small, the elastic strain rate $\mathbf{D}^e$ is described by the hypoelastic law

$$\mathbf{D}^e = \mathscr{L}_e^{-1} \overset{\nabla}{\boldsymbol{\sigma}}, \tag{2}$$

in terms of the Jaumann derivative of the Cauchy stress tensor $\boldsymbol{\sigma}$, $\overset{\nabla}{\boldsymbol{\sigma}} = \dot{\boldsymbol{\sigma}} - \mathbf{W}\boldsymbol{\sigma} + \boldsymbol{\sigma}\mathbf{W}$, where $\mathbf{W}$ the continuum spin tensor. Here, $\mathscr{L}_e$ is taken as the standard fourth-order tensor of isotropic elastic moduli with Cartesian components

$$\mathscr{L}_{ijkl} = \frac{E}{2(1+\nu)}\left[\left(\delta_{ik}\delta_{jl} + \delta_{il}\delta_{jk}\right) + \frac{2\nu}{1-2\nu}\delta_{ij}\delta_{kl}\right], \tag{3}$$

where E is Young's modulus and ν is Poisson's ratio (G is the corresponding shear modulus).

According to the Argon (1973) model for plastic flow in amorphous polymers, the equivalent plastic shear strain rate $\dot{\gamma}^p$ due to an applied shear stress τ is given by

$$\dot{\gamma}^p = \dot{\gamma}_0 \exp\left[-\frac{As_0}{T}\left(1 - \left(\frac{\tau}{s_0}\right)^{5/6}\right)\right], \tag{4}$$

where $\dot{\gamma}_0$ and A are material parameters, T is the absolute temperature, and so is the material shear strength. In order to incorporate the effect of pressure p on the plastic flow, and the effect of strain softening, s_0 in Eq. (4) is replaced with $s + \alpha p$ with α being the pressure sensitivity parameter. The current shear strength s is assumed to evolve with plastic straining from its initial value s_0 at initial yield via

$$\dot{s} = h(1 - s/s_{ss})\dot{\gamma}^p, \tag{5}$$

in which h is a material parameter characterizing the rate of softening and s_{ss} is the saturation value of s. The shear rate according to Eq. (4) determines the plastic strain rate tensor $\mathbf{D}^p$ through

$$\mathbf{D}^p = \dot{\gamma}^p \mathbf{N}, \tag{6}$$

where **N** is the deviatoric part $\bar{\boldsymbol{\sigma}}'$ of the driving stress $\bar{\boldsymbol{\sigma}}$, normalized by the effective equivalent shear stress τ,

$$\mathbf{N} = \frac{\bar{\boldsymbol{\sigma}}'}{\sqrt{2}\,\tau}, \quad \tau = \sqrt{\frac{1}{2}\bar{\boldsymbol{\sigma}}' \cdot \bar{\boldsymbol{\sigma}}'}. \tag{7}$$

Here, the driving stress $\bar{\boldsymbol{\sigma}}$ is defined by

$$\bar{\boldsymbol{\sigma}} = \boldsymbol{\sigma} - \mathbf{b}, \tag{8}$$

where **b** is the back stress tensor accounting for the strain hardening of the material.

Strain hardening in amorphous polymers is due to the stretching and simultaneous rotation of the molecular chains in the underlying network upon yield. Following the original suggestion of Haward and Thackray (1968), this deformation-induced, so-called orientational hardening is described by back stress whose description is based on the analogy with rubber elasticity. The back stress **b** is formulated in terms of its principal components b_α on the unit principal direction $\mathbf{e}_\alpha^{\mathrm{p}}$ of the left plastic stretch tensor, in terms of the corresponding principal plastic stretches λ_α, as follows:

$$\mathbf{b} = \sum_\alpha b_\alpha(\mathbf{e}_\alpha^{\mathrm{p}} \otimes \mathbf{e}_\alpha^{\mathrm{p}}), \quad b_\alpha = b_\alpha(\lambda_\beta). \tag{9}$$

To avoid confusion, principal tensor components and the corresponding eigenvectors are denoted with Greek indices, for which the summation convention is not implied. The description used here, was proposed by Wu and Van der Giessen (1993) on the basis of their description of the fully 3D orientation distribution of molecular chains in a non-Gaussian network. They showed that their numerical computations can be captured very accurately by the following combination of the classical three-chain network description and the recent Arruda and Boyce (1993) eight-chain model:

$$b_\alpha = (1-\rho)\,b_\alpha^{3-\mathrm{ch}} + \rho\, b_\alpha^{8-\mathrm{ch}} \tag{10}$$

with ρ being determined by the maximum plastic stretch $\bar{\lambda} = \max(\lambda_1, \lambda_2, \lambda_3)$ through $\rho = 0.85\bar{\lambda}/\sqrt{N}$. Here, N is a statistical parameter, which determines the limit stretch $\lambda_{\max}$ of a molecular chain as $\lambda_{\max} = \sqrt{N}$. The principal back stress components in Eq. (10) are given by

$$b_\alpha^{3-\mathrm{ch}} = \frac{1}{3} C^{\mathrm{R}} \sqrt{N}\, \lambda_\alpha \mathscr{L}^{-1}\left(\frac{\lambda_\alpha}{\sqrt{N}}\right) \tag{11}$$

$$b_\alpha^{8-\mathrm{ch}} = \frac{1}{3} C^{\mathrm{R}} \sqrt{N}\, \frac{\lambda_\alpha^2}{\lambda_{\mathrm{c}}} \mathscr{L}^{-1}\left(\frac{\lambda_{\mathrm{c}}}{\sqrt{N}}\right); \quad \lambda_{\mathrm{c}}^2 = \frac{1}{3}\sum_{\beta=1}^{3} \lambda_\beta^2, \tag{12}$$

where C^{R} is a material constant and $\mathscr{L}^{-1}$ is the inverse of the Langevin function $\mathscr{L}(\beta) = \coth\beta - 1/\beta$. As in previous studies (Wu and Van der Giessen, 1994, 1995, 1996), it is assumed that the elastic strains remain small enough to approximate the plastic stretches λ_α to be substituted into Eqs. (11) and (12) by the total principal stretches. When the value of either λ_α or λ_{c} approaches the chain limit stretch $\lambda_{\max}$, the hardening rate provided by the increased network stiffness accelerates enormously, thereby suppressing effectively all further plastic flow, and the network 'locks'. Therefore, when either λ_α or λ_{c} exceeds $0.99\lambda_{\max}$, viscoplastic flow is disabled ($\dot{\gamma}^{\mathrm{p}} = 0$), so that $\mathbf{D}^{\mathrm{p}} = \mathbf{0}$ and the instantaneous response becomes fully elastic. Rupture of any type is not accounted for in the present model. Also, thermal effects on hardening and rate effects through self-heating (see, e.g., Arruda et al., 1995) are not included here since the computations have been confined to isothermal situations.

With Eqs. (1), (2) and (6) the final constitutive equations are obtained in the form

$$\overset{\nabla}{\boldsymbol{\sigma}} = \mathscr{L}_{\mathrm{e}} \boldsymbol{D} + \dot{\boldsymbol{\sigma}}_{\mathrm{v}} \tag{13}$$

with $\dot{\boldsymbol{\sigma}}_{\mathrm{v}} = -\dot{\gamma}^{\mathrm{p}}(\sqrt{2}\,G/\tau)\bar{\boldsymbol{\sigma}}'$. This constitutive model has been successfully applied to predict many aspects of the large plastic deformation behavior of glassy polymers observed in experiments. In particular, it is capable of describing the initiation and propagation of localized shear bands that typically occurs in these materials, and which are responsible for e.g. neck propagation during tension (cf. e.g., Wu and Van der Giessen, 1994, 1995, 1996; Arruda et al., 1995).

3. Problem definition and method of analysis

Any actual crack tip has a finite root-radius. Even when an initially sharp crack is assumed, the tip of the crack will be blunted after a certain amount of loading is exerted. Indeed, numerical experiments based on initially sharp crack tips showed that severe blunting took place in the very early stages of crack tip plasticity, leading to a highly distorted mesh. Therefore, we consider here an initially blunted crack with a root radius r_t. Confining attention to the framework of small-scale yielding, the boundary layer approach is employed to study the Mode I plane strain fields near a stationary crack. Isothermal conditions are assumed. A circular region surrounding the crack tip is considered, where, because of symmetry about the crack plane, only half of the geometry needs to be analyzed, as depicted in Fig. 2. The remote elastic field for an applied stress intensity factor K_I is prescribed along the circular arc in terms of the displacement components u_1, and u_2 in the Cartesian frame x_i according to

$$u_1 = 2(1+\nu)\frac{K_I}{E}\sqrt{\frac{r}{2\pi}}\cos\frac{\theta}{2}\left[2-2\nu-\left(\cos\frac{\theta}{2}\right)^2\right], \tag{14}$$

$$u_2 = 2(1+\nu)\frac{K_I}{E}\sqrt{\frac{r}{2\pi}}\sin\frac{\theta}{2}\left[2-2\nu-\left(\cos\frac{\theta}{2}\right)^2\right], \tag{15}$$

where r and θ are polar coordinates with the origin located at the crack tip. Loading is prescribed to take place at a constant loading rate $\dot{K}_I$. The remaining boundary conditions are traction-free conditions on the crack surface and symmetry boundary conditions along $x_2 = 0$, $x_1 \geq 0$.

A finite strain, quasi-static finite element analysis of the full-field, near-tip problem is carried out, using a Total Lagrangian description of the field equations. The formulation is similar to that employed in previous finite element studies with the same material model (Wu and Van der Giessen, 1994, 1995, 1996). The solution of the problem is obtained on the basis of a linear incremental form of the virtual work principle. The solution procedure employs an equilibrium correction procedure, an adaptive time stepping method and makes use of a rate tangent form of the constitutive Eq. (13); details may be found in (Wu and Van der Giessen, 1996) and will not be repeated here. Quadrilateral elements are used, each of which is built up of four linear velocity, triangular subelements arranged in a 'crossed triangle' configuration. It is well-known that with a proper aspect ratio and orientation these elements are well suited to pick up localized deformation. Fig. 2 shows the finite element mesh used in a number of analyses to be presented. This mesh is quite refined near the notch, using 32 elements along half the notch radius. Most of the results to be resented have been obtained with an even finer mesh that has 52 elements along the half radius, but with otherwise similar characteristics.

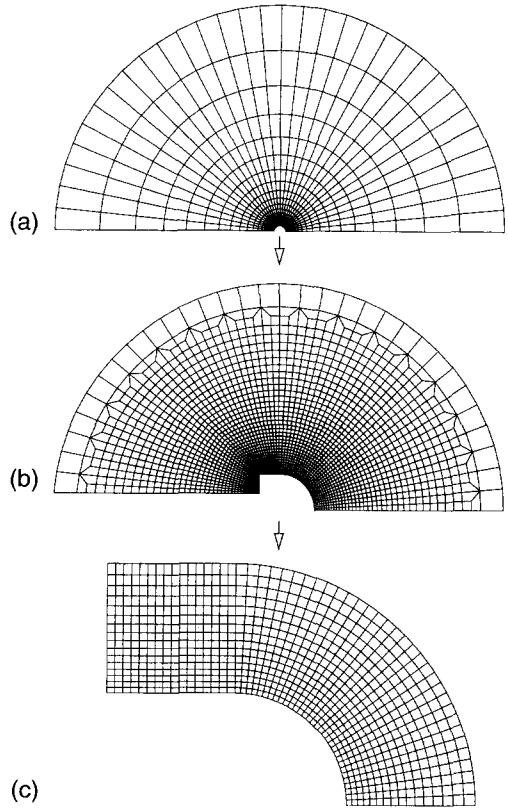

Fig. 2. Geometry of the problem studied and finite element mesh used in the analysis. (a): outer mesh; (b): inner mesh; (c): near-tip mesh. This mesh has 32 elements along the half notch radius. A second, refined mesh uses 52 elements instead.

Table 1
Material parameters

Material	ν	E/s_0	s_{ss}/s_0	As_0/T	α	h/s_0	N	C^R/s_0
A	0.4	9.38	1	79.2	0.08	0	100	0
B	0.4	9.38	1	79.1	0.08	0	2.8	0.309
c	0.4	9.38	0.79	79.2	0.08	5.15	2.8	0.132
D	0.4	9.38	0.45	79.2	0.08	1.10	2.8	0.132
E	0.4	9.38	0.79	79.2	0.08	5.15	100	0

4. Results and discussion

In order to gain an understanding of how the constitutive behavior influences the plastic deformation processes near the crack tip in glassy polymers, a parameter study is presented here. A total of five sets of material parameters is considered, as listed in Table 1. The sets differ mainly in the material parameters s_{ss}, h, N and C^R that govern the softening and hardening characteristics, since these are the key features of amorphous polymers. Even though these parameters are considered as constants in the model, their values for actual materials may depend on strain-rate and temperature. Hence, the values in Table 1 can be regarded to apply to different materials or to different conditions.

The uniaxial stress–strain behavior for each of these materials is displayed in Fig. 3 for the purpose of reference. Material A is chosen to be the reference material, which exhibits elastic perfectly-plastic behavior. Material B exhibits no softening but progressive hardening after yielding; this gives a uniaxial response that is akin to that of some semi-crystalline polymers. The constitutive behavior of material C is representative of PC at room temperature ($T = 294$ K), which undergoes intrinsic softening after yielding, followed by a progressive strain hardening (apart from an inconsequential difference in the value of Poisson's ratio ν, this parameter set corresponds to that used in (Wu and Van der Giessen, 1996)). Material D has the same hardening parameters (N and C^R/s_0) as material C, but exhibits stronger softening due to a smaller value of s_{ss}/s_0 (this is characteristic of certain grades of SAN). The value of h is reduced in order that the initial slope of softening, $h(1 - s_0/s_{ss})$, remains the same. Contrary to material B, material E is another limiting case with the same softening behavior as material C but no progressive hardening. It should be noted in Fig. 3 that the actual yield stress for material E is somewhat lower than for the others; this is due to the fact that this stress level is weakly dependent on C^R since we assume the back stress to be determined by the total stretch. With reference to the schematic in Fig. 1, the chosen parameter values scan a range of values of the stress drop, $\tau_y - \tau_{min}$ and the shear band strain γ_b during shearing.

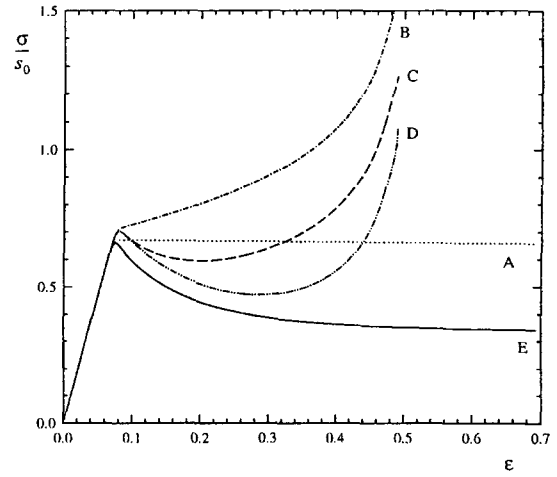

Fig. 3. True stress σ versus logarithmic strain ε curves in uniaxial tension at $\dot{\varepsilon} = 10^{-3}$ for the different material parameters listed in Table 1.

In all cases, the value of E/s_0 is chosen on the basis of typical values of the yield stress and the yield strain in uniaxial tension. Thus, in fact, E is not equal to the initial Young's modulus of amorphous polymers since they typically show a small strain viscoelastic effect prior to yield, which is now 'lumped' into a reduced value of s_0/E (cf. Wu and Van der Giessen, 1994).

Even though the material is essentially rate dependent, our focus here is not on material rate effects. It is assumed here that the material model described in the previous section is valid for the whole range of strain-rates encountered around the crack tip. With this model, a change in the rate of deformation primarily influences the shear strength, and thus basically leads to a simple vertical shift in the stress–strain response of Fig. 3 (see e.g., Wu and Van der Giessen, 1994). Hence, the fields are not affected much by the applied strain-rate other than through a scaling factor. Therefore, all cases have

simply used the same value $\dot{K}_I/\dot{\gamma}_0 s_0\sqrt{r_t} = 5.67 \times 10^{-16}$ in Eqs. (14) and (15).

To fix ideas, consider a standard single edge notched (SEN) specimen of PC with an initial notch tip radius of 0.1 mm. Using typical values of $\dot{\gamma}_0 = 2 \times 10^{15}$ s^{-1} and $s_0 = 97$ MPa for PC (from Wu and Van der Giessen, 1993), the mentioned normalized loading rate corresponds to $\dot{K}_I = 1.1$ MPa$\sqrt{\text{m}}\,s^{-1}$. This value is consistent with a displacement rate on the order of 10^{-4} m/s in the remote region of the specimen (about 20 mm from the crack tip), in which case isothermal deformation is usually assumed.

4.1. Plastic zone

As mentioned before, plastic deformation takes place by the initiation and subsequent propagation of bands of localized plastic shearing. Therefore, we present the numerical results of the active crack-tip plastic zone by plotting contours of the instantaneous plastic shear rate $\dot{\gamma}^p$. They are conveniently normalized by a 'strain rate' quantity $\dot{\Gamma}$ defined by

$$\dot{\Gamma} = \frac{\dot{K}_I}{s_0\sqrt{r_t}}, \tag{16}$$

while all coordinates are normalized by the initial root-radius of the notch tip, r_t.

For a material exhibiting elastic perfectly-plastic behavior, such as material A, the crack-tip plastic zone at a typical level of K_I, is shown in Fig. 4. It can seen that this type of material displays a kidney-shaped plastic zone around the crack tip, which is well known for metals. The maximum plastic shear rate occurs at the crack tip and extends along the crack surface when the load increases. For materials with progressively increasing hardening after yielding, like material B, the outer boundary of the plastic zone still resembles that in metals (see Fig. 5). However, due to the increasing hardening at the crack tip, the plastic shearing at the crack tip decreases with increasing loading and finally dies out. As a result, the maximum $\dot{\gamma}^p$ propagates from the crack tip upwards along the crack surfaces. A comparison of area and magnitude of the plastic zones in Fig. 4 and Fig. 5 (note that both snapshots are at about the same K_I) indicates that increasing strain

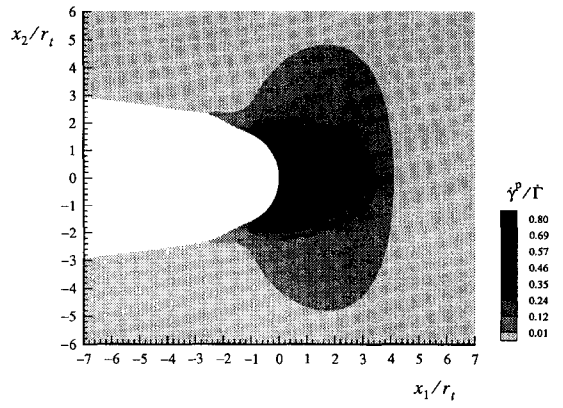

Fig. 4. Crack-tip plastic zone in material B at $K_I/s_0\sqrt{r_t} = 4.24$. The bottom half of the displayed region is a simple mirror image of the top half that is actually analyzed, in order to better show the shear band patterns.

hardening also tends to depress both extent and intensity of the plastic activity near the crack tip.

Fig. 6 shows the development of the crack-tip plastic zone in material C, which exhibits both softening and hardening after yielding. The snapshots in this figure at three stages of the applied loading history show a completely different shape of the plastic zone than in materials A and B. The intrinsic softening is seen to intensify and localize the plastic deformation near the crack tip, as indicated by the relatively sharp shear bands and larger value of the maximum plastic shear rate $\dot{\gamma}^p$. Due to the increasing hardening of the material, the shear bands propagate away from the tip region, where the plastic

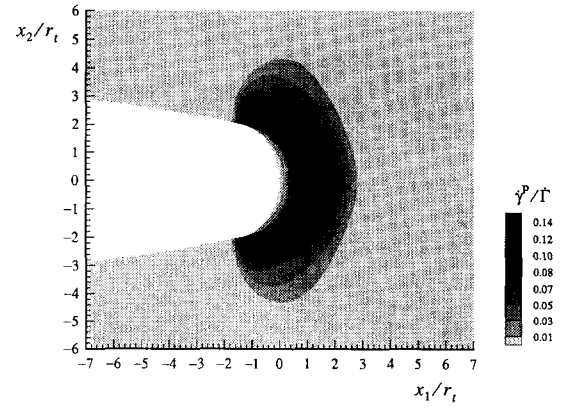

Fig. 5. Crack-tip plastic zone in material B at $K_I/s_0\sqrt{r_t} = 4.34$.

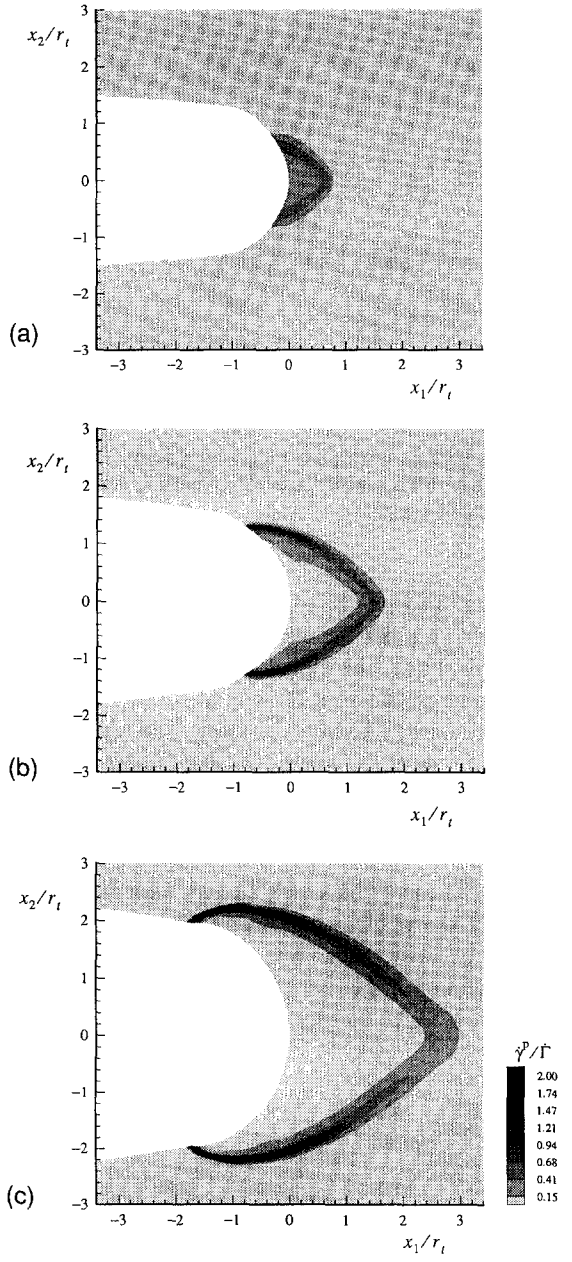

Fig. 6. Crack-tip plastic zones in material C at (a): $K_I / s_0\sqrt{r_t} = 1.77$, (b): $K_I / s_0\sqrt{r_t} = 2.75$ and (c): $K_I / S_0\sqrt{r_t} = 4.24$. The results have been obtained using the fine mesh.

activity decreases and finally vanishes (cf. Fig. 6a, b). With increasing loading, the current plastic zone grows in an almost self-similar manner, with the origins of the shear bands on the crack surface propagating in the negative x_1 direction, and the tip of the plastic zone (where shear bands cross) moving in the forward direction away from the tip. There is a slight tendency, however, for the plastic zone to become more and more elongated. This is reflected in the angle between shear bands. Already at an early stage (Fig. 6a), this angle is less than 90°, and it is seen to decrease with increasing load until a value of 77° in Fig. 6c. To fix ideas, the actual value of the applied stress intensity factor, using the typical values for PC mentioned above, corresponding to Fig. 6c is $K_I = 4.11$ MPa$\sqrt{\text{m}}$. Although this value is high compared with the critical stress intensity factor, $K_c = 2.24$ MPa$\sqrt{\text{m}}$, for crack initiation in PC specimens (Parvin and Williams, 1975), it is still considered here, simply for the purpose of studying the development of the plastic zone with increased loading; as mentioned before, actual fracture is not discussed here.

In view of the intrinsic softening of the material C (see Fig. 3), it is to be expected that the localization of deformation demonstrated above is sensitive to the mesh. On the other hand, it should be realized that the material response is also rate-dependent, which tends to suppress the pathological mesh dependence of rate-independent solids (see Needleman, 1988). For quasi-static problems as considered here, the strain-rate dependence tends to limit the shear band width, by virtue of the fact that the rate-dependency counteracts the reduction of the shear stress within a shear band upon intrinsic softening. These matters have been investigated by re-analyzing the problem with several meshes. It was found that the results, including shear band widths, obtained with the fine version of the mesh (used in Fig. 6) agreed well with those found with the coarser mesh depicted in Fig. 2. The initiation of new shear bands with the chosen elements is well-known to be somewhat sensitive to the orientation of the element diagonals. In the present problem with the continuous nucleation of new shear bands, it is impossible to ensure optimal element orientations at all stages. However, we have carefully tuned the gradation in the element size away from the notch surface so that the mesh orientation in the deformed configuration has a small influence on the shear band propagation.

Let us now consider material D with a stronger softening than material C, i.e. a lower value of s_{ss}/s_0, but with the same hardening parameters as material C. A more complicated pattern of the plastic zone can be seen in Fig. 7, in which four snapshots during the deformation history are included to show the development of the plastic zone near the crack tip with increasing K_I. Fig. 7a shows the plastic zone at an early stage of the process. One sees that the shear bands emanating from above and below the crack plane cross over ahead of the tip. As loading is increased, these shear bands propagate in qualitatively the same manner as seen above. However, since softening is much stronger for this material than for material C, two new families of shear bands get initiated outside of the previous plastic zone at some point, as shown in Fig. 7b. At higher loading levels, as shown in Fig. 7c, d, even more shear bands are activated, giving rise to a 'fan' of active shear bands that begins to show some similarity with the Rice and Johnson (1970) slip line solutions around a blunted crack tip. It is clear from these pictures that plastic flow of the material contained inside the plastic zone in the vicinity of the crack tip has stopped, because of hardening. The development of the plastic zone in this case obviously is not in a near self-similar manner as before. Although the angle between the shear bands near the tip of the plastic zone is not well-defined in this case, it seems that the angle is very close to 90° in Fig. 7a, b, but increases with increasing load levels to a value of around 100° at the stage shown in Fig. 7d.

From the previous results, we have seen that (intrinsic) softening and orientational hardening are two counteracting factors influencing crack-tip plastic deformation. Softening tends to intensify the lo-

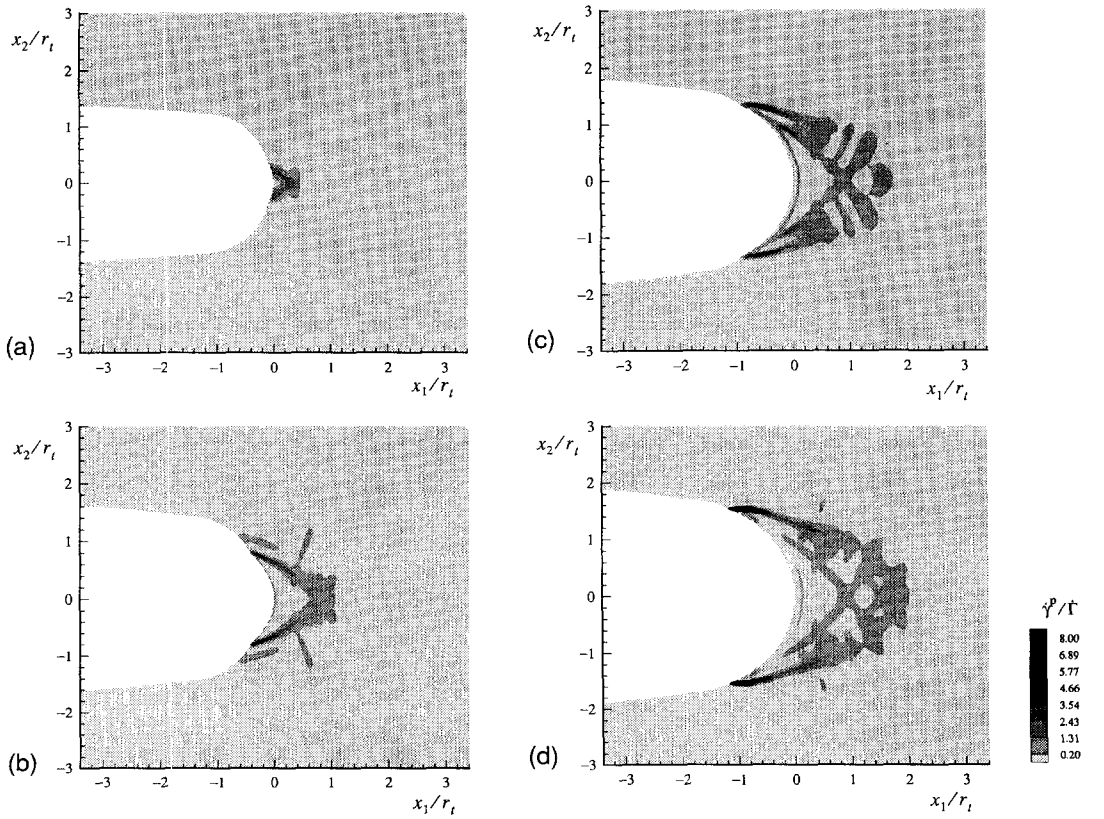

Fig. 7. Crack-tip plastic zones in material D at (a): $K_I/s_0\sqrt{r_t} = 1.37$, (b): $K_I/s_0\sqrt{r_t} = 2.18$, (c): $K_I/s_0\sqrt{r_t} = 2.78$ and (d): $K_I/s_0\sqrt{r_t} = 3.05$. The results have been obtained using the fine mesh.

calization of plastic deformation, while the increasing strain hardening depresses the local plastic shearing process and governs the propagation of shear bands. Fig. 4 gives an example of the plastic zone in a material where only hardening after yielding is present; Figs. 5–7 demonstrate the coupled effect of softening and hardening on the plastic deformation in front of the crack tip. In order to better examine the softening effect, Fig. 8 considers a limiting case, material E, which exhibits no hardening but only softening after yielding. From the early stages, Fig. 8a, the plastic zone comprises multiple shear bands. More and more new shear bands are activated with increasing loading, Fig. 8b, c, but no shear band propagation takes place because of the absence of hardening. Instead, the deformation inside each band continues to accumulate since the value of γ_b (see Fig. 1) is unbounded. Thus, the stress concentration near the crack tip in material E is relaxed by localization in many shear bands that show a definite similarity with slip lines, while in material C all plastic relaxation is localized in a single family of shear bands. As a consequence, the plastic shear rate $\dot{\gamma}^p$ inside the shear bands in material E remain significantly lower than that observed for materials D and C in Figs. 7 and 6, respectively. The angle between shear bands in material E is roughly equal to 100°, as in material D, independent of the load level. Finally we note from Fig. 8 that the formation of multiple shear bands leads to the development of waviness on the notch surface.

4.2. Mean normal stress

The types of polymers for which the constitutive model used here is applicable, often fail by crazing.

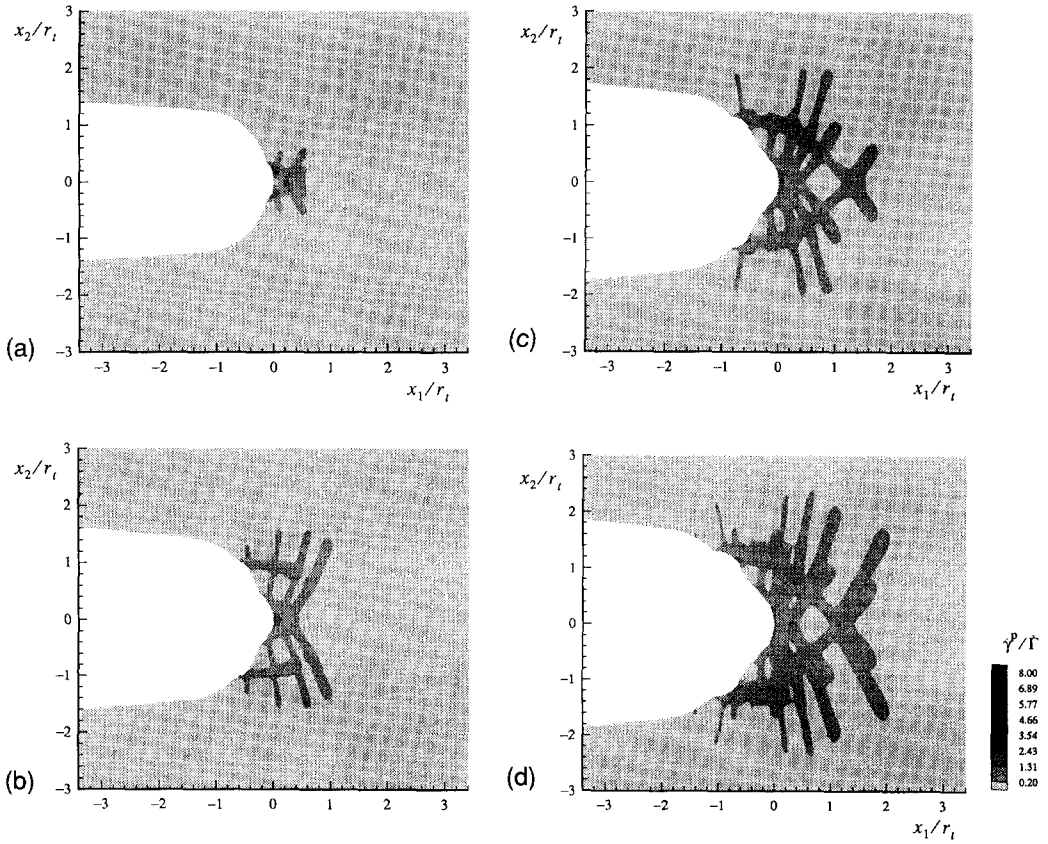

Fig. 8. Crack-tip plastic zones in material E at (a): $K_I/s_0\sqrt{r_t} = 1.45$, (b): $K_I/s_0\sqrt{r_t} = 2.12$, (c): $K_I/s_0\sqrt{r_t} = 2.50$ and (d): $K_I/s_0\sqrt{r_t} = 2.85$. The results have been obtained using the fine mesh.

Although the crazing mechanism has not been fully understood, the mean normal (hydrostatic) stress $\sigma_m = \frac{1}{3}\mathrm{tr}\,\boldsymbol{\sigma}$ is believed to play an important role in the initiation of crazes (e.g. Argon and Hannoosh, 1977; Kramer, 1983). A thorough study of crazing mechanisms in combination or competition with plasticity does not seem possible at this stage and is outside the scope of this paper. However, it does seem pertinent to study the distribution of the mean stress in the crack tip region and how it is influenced by the plastic deformation. These results may be instrumental for future research into the crazing mechanisms in glassy polymers.

It is not intended here to show the mean stress distributions for all materials considered in the foregoing. In view of the plastic zones observed before, we consider two typical cases, which lead to the single set of shear bands (material C) and multiple sets of shear bands (material E), respectively. Fig. 9a, for material C, shows how the occurrence of shear bands relax the elastic mean stress distribution at the tip of the notch. This leaves a mean stress peak at some distance ahead of the crack tip, which moves as the load increases and the shear bands propagate, as shown in Fig. 9b. Careful comparison with the shear band patterns in Fig. 6 reveal that the maximum value of σ_m is located at (or slightly ahead) of the location where the shear bands cross.

Fig. 10 shows the mean stress distributions in the material E at the same stages of loading as in Fig. 8. Associated with the development of multiple shear bands, quite different mean stress distributions are observed as in Fig. 9. Initially (Fig. 10a) the maximum value of σ_m occurs ahead of the tip near the intersection of the two main shear bands. As the load is increased and new shear bands are being formed, mean stress peaks are sometimes found at some offset from the crack plane at various crossing locations of shear bands, as clearly seen in Fig. 10b, while at other stages the peak values are found straight ahead of the tip (Fig. 10c).

To elucidate the process of propagation of the mean stress peaks during the loading process, Figs. 11 and 12 show the evolution of the distribution ahead of the tip along the crack plane for materials C and E, respectively. The mean stress peak in material C is seen in Fig. 11 to steadily propagate in the x_1, direction, while its value monotonically increases

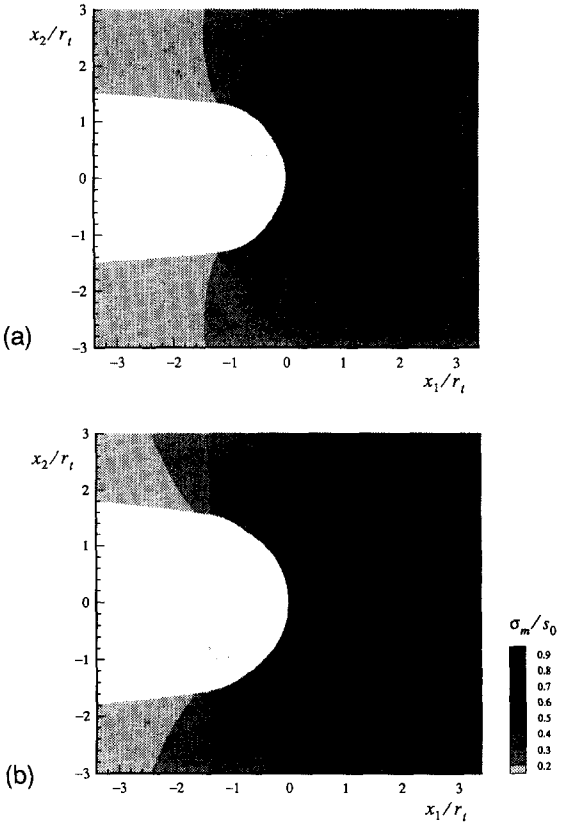

Fig. 9. Distribution of the mean normal stress in material C, normalized by the initial shear strength s_0, at (a): $K_I/s_0\sqrt{r_t} = 1.77$, (b) $K_I/s_0\sqrt{r_t} = 2.75$ (cf. Fig. 6).

and seems to approach a limiting value of around $1.25s_0$ at the last stages shown (corresponding to about 2.68 times the original notch radius). Inside the plastic zone, very close to the tip of the crack, the mean stress fields are akin of the elastic near-singular fields. This is to be attributed to the fact that the material in that region has been deformed far beyond the point marked γ_b in Fig. 1, and approaches the limit stretch of the entangled molecular net-work where the material is taken to lock. Hence, the instantaneous behavior of this material is close to elastic again, thus explaining the near-singular behavior. The intensity of the 'singular' mean stress fields very near the tip are obviously much reduced in comparison with the far field intensity by virtue of relaxation in the plastic zone. Contrary to this phenomenology, the maximum value of the mean stress

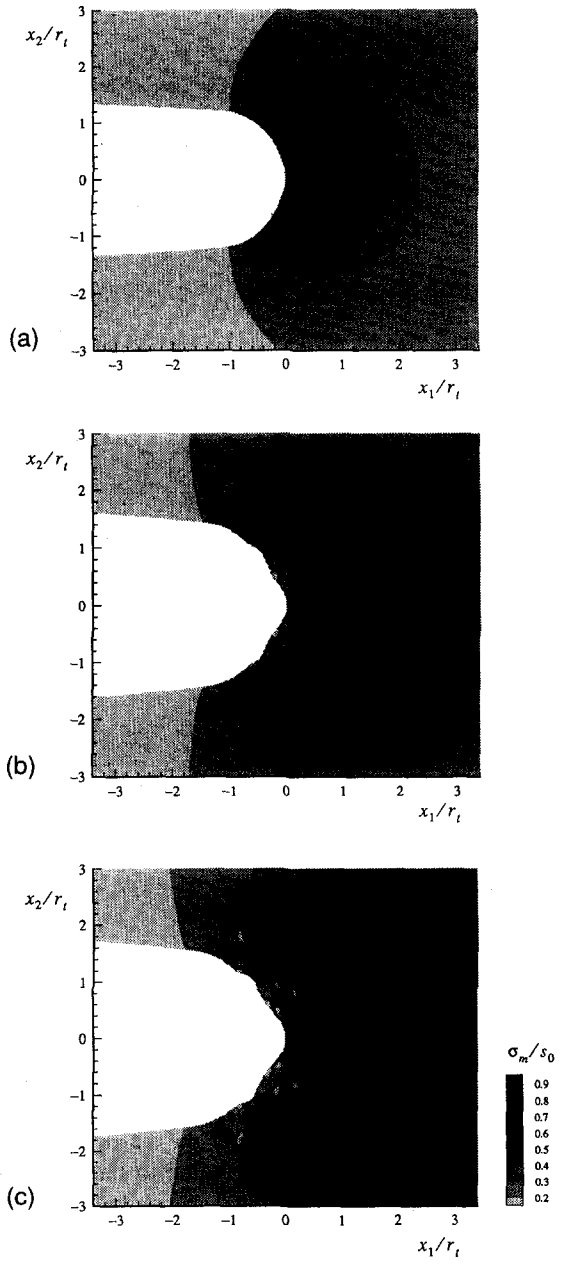

Fig. 10. Distribution of the normalized mean stress in material E at (a): $K_I/s_0\sqrt{r_t} = 1.45$, (b): $K_I/s_0\sqrt{r_t} = 2.12$ and (c): $K_I/s_0\sqrt{r_t} = 2.50$ (cf. Fig. 8).

at any load level in material E, depicted in Fig. 12, always occurs at some distance ahead of the crack tip. Due to the absence of any hardening, locking of the network cannot occur. The location of the mean

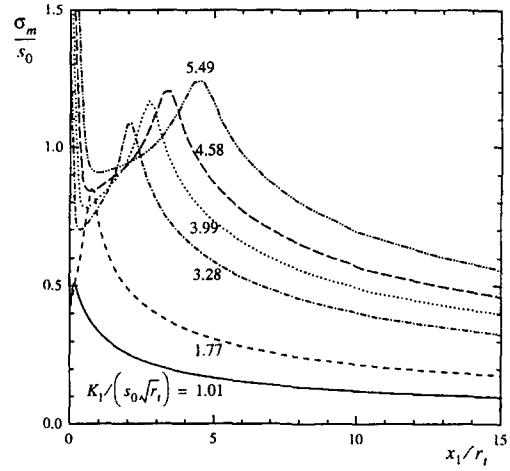

Fig. 11. Mean stress distributions along the crack plane $x_2 = 0$ in material C at various loading stages (cf. Fig. 9).

stress peak is not defined precisely when multiple shear band families are active, as mentioned earlier in relation to Fig. 10. It is interesting to note, both from Figs. 11, 12 and Figs. 9, 10, that the mean stress values at the peak locations in the two materials at the same load level are the same to a fair accuracy.

4.3. Crack-tip opening displacement

Theoretical as well as experimental work on metals has revealed (cf., e.g. McMeeking, 1977 and

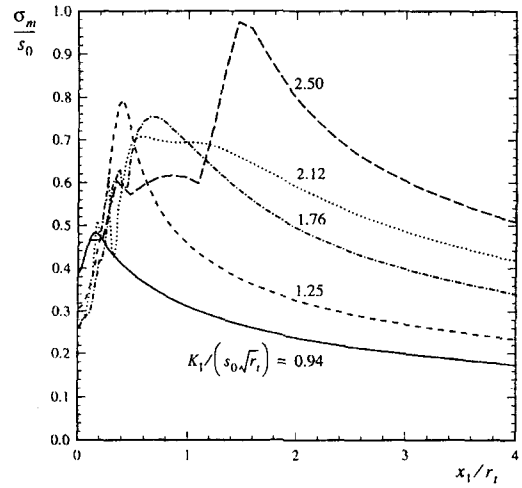

Fig. 12. Mean stress distributions along the crack plane $x_2 = 0$ in material E at various loading stages (cf. Fig. 10).

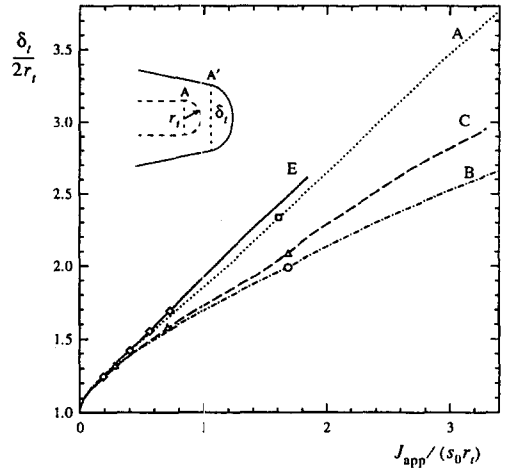

Fig. 13. Crack-tip opening displacement δ_t versus applied J-integral, J_{app} for different materials. Markers indicate the loading stages at which the crack-tip plastic zone is displayed previously for these materials.

references contained therein) that the crack tip opening during small-scale yielding is proportional to the applied value of the J-integral (Rice, 1968) to a fair degree of accuracy.

Here we examine how the softening and hardening behavior of glassy polymers influence the crack-tip opening displacement δ_t. Following McMeeking (1977), δ_t is defined as the distance between the two nodes lying at the intersections of the straight flank and the semicircular tip of the undeformed notch. The applied J-integral, J_{app}, is determined from the small-scale yielding expression

$$J_{app} = (1 - \nu^2) K_I^2 / E. \tag{17}$$

Fig. 13 displays the crack opening displacement, normalized by the initial crack-tip opening, versus J_{app} for materials A, B, C and E. For small values of J_{app}, the curves for all materials collapse onto a single parabolic-like curve, indicating that crack opening is dominated by elastic deformations so that δ_t is proportional to $\sqrt{J_{app}}$. Clearly, elasticity plays a much more important role than in metals since the yield strains can be as large as 10% or so (cf. e.g., Fig. 3). Apart from this initial curvature, the δ_t versus J_{app} curve for material A (without hardening and without softening) is linear up to large load levels. For material B, the slope of the curve is considerably lower than for A, as expected for a hardening material (McMeeking, 1977), but also the curve deviates more from proportionality. For material C that additionally shows intrinsic softening, the slope is in between those of A and B, which demonstrates that the opening of the crack is controlled by the concurrent actions of softening and strain hardening within the plastic zone. The δ_t versus J_{app} curve for material E deviates only slightly from the reference material A, even though the stress drop due to softening can be of the order of 50% depending on strain-rate, as seen in Fig. 3. This can be attributed to the fact that the yielded and softened material inside the plastic zone has such a low stress-carrying capacity that the 'effective crack tip', as far as the opening of the crack is concerned, coincides with the current front of the plastic zone.

5. Conclusions

The crack-tip plastic zones in glassy polymers have been studied in this paper using a constitutive model for such materials that incorporates their typical softening and hardening behavior. It is found that the intrinsic softening makes the shape of the crack-tip plastic zone in glassy polymers different from that for metals, as contained for instance in the HRR field. Softening and hardening are two counteracting factors influencing crack-tip plastic deformation. Generally speaking, softening tends to intensify the localized plastic deformation, while hardening depresses the local plastic shearing process. For materials with no softening the plastic zone in front of the crack tip is qualitatively similar to that in metals, even though the hardening response in the two materials are different. For polymers with some extent of softening and hardening, a single set of shear bands initiated at the crack tip will continuously propagate and expand in an almost self-similar manner with increasing loading, leading to typical plastic zones as in Fig. 6b. With sufficiently strong softening or weak hardening, the material undergoes plastic deformation in front of the crack tip in the form of multiple families of shear bands, as shown in Fig. 8c. This type of plastic zone shows similarity with the slip-lines around blunted crack tips (Rice and Johnson,

1970). Both latter types of plastic zones have been observed in some polymers (Jeong et al., 1994; Ishikawa, 1995).

Care should be taken, however, in comparing the model predictions with experimental results. First of all, one needs to be aware of possible two different concepts of 'plastic zones'. The experimental visualization of plastic zones is based on the change in birefringence caused by the molecular reorientation during previous plastic flow; here, we have used the term plastic zone in relation with regions of currently active plasticity. Secondly, depending on size scale and material, micrographs often show individual micro shear bands that are organized in more macroscopic bands (e.g., Jeong et al., 1994). The continuum model used in this study can at best given a continuum representation of micro shear bands and describe their collective behavior (note from Eq. (7) that plasticity is determined by a modified J_2-like stress invariant τ). The model-based shear bands obtained here should be interpreted as such macroscopic bands; any internal structure in the bands cannot be resolved.

An interesting property of the plastic zone observed here is the angle between crossing shear bands. As pointed out by Jeong et al. (1994), the angle between slip lines around a notch is 90° according to the classical solution (Rice and Johnson, 1970) for a pressure independent material, but is reduced (under tensile loading) by an amount $\sin^{-1}\alpha$ for pressure dependent materials with pressure dependence parameter α. For the value $\alpha = 0.08$ used in all computations reported here, this angle is reduced by 4.6°. The present computations indicate a more complex phenomenology where the change in angle between shear bands depends on the softening and hardening parameters, and can either be positive or negative. In a case that led to a single family of shear bands, Fig. 6, the angle was smaller than 90° by an amount of around 13°, whereas cases with stronger softening or less hardening leading to multiple shear bands, the angle was larger by around 10°.

In relation to the role of crack tip plasticity during failure of polymers, this study has demonstrated two aspects. First of all, it has been found that the distribution of mean normal stresses is intimately related to the pattern of plastic deformation in front of the crack. The maximum mean stress is found to occur near the tip of the plastic zone where shear bands cross, i.e. at some distance ahead of the tip. This agrees qualitatively with the position at which crazes have been observed to initiate experimentally in amorphous polymers (Yamamoto and Furukawa, 1995) and in polymer blends (Ishikawa, 1995). The level of this peak mean stress σ_m increases with increasing remote loading, up to a value of about $1.25 s_0$ for typical material parameters (material C). This seems to be lower than the typical values found for metal plasticity by McMeeking (1977). In making the comparison it should be realized that the present material model accounts for rate-dependent flow: for very high strain rate, the Von Mises yield stress σ_0 approaches $\sqrt{3}\, s_0$ (neglecting pressure sensitivity) so that the steady state mean stress is only $0.7\sigma_0$; for the strain rate in Fig. 3 we see that $\sigma_0 = 0.7 s_0$ so that $\sigma_m = 1.8\sigma_0$. This deviation from McMeeking's (1977) result is to be attributed to the localized plastic flow, which tends to reduce the constraints responsible for the relatively high mean stress in hardening solids. The effect is only mildly related to the pressure sensitivity of the material; Jeong et al. (1994) have developed the slip line solution for pressure sensitive materials, which implies that the maximum mean stress is reduced by only 15% when a pressure dependence of $\alpha = 0.08$ is introduced. Secondly, in materials that show strain hardening following the intrinsic softening, we find that 'locking' takes place in the material next to the notch tip which has previously deformed plastically and is now contained inside the plastic zone. In that case, when moving away from the tip of the notch, we first encounter a plasticity-free zone before reaching the plastic zone. This is in a sense analogous to the idea of a dislocation-free zone that has been advanced for metals by Suo et al. (1993). Obviously, this locked region is shielded from the remote elastic field by the plastic zone, but severe stress concentration takes place. It is conceivable that these stress concentrations lead to cleavage fracture in materials that are sufficiently resistant to crazing.

Acknowledgements

This work is part of a research program of the "Stichting voor Fundamenteel Onderzoek der Ma-

terie (FOM)'', which is financially supported by the ''Nederlandse Organisatie voor Wetenschapplijk Onderzoek (NWO)''.

References

Argon, A.S. and J.G. Hannoosh (1977), Initiation of crazes in polystyrene, *Philos. Mag.* 36, 1195–1216.

Argon, A.S. (1973), A theory for the low-temperature plastic deformation of glassy polymers, *Philos. Mag.* 28, 839–865.

Arruda, E.M. and M.C. Boyce (1993), A three-dimensional constitutive model for large stretch behavior of rubber materials, *J. Mech. Phys. Solids* 41, 389–412.

Arruda, E.M., M.C. Boyce and R. Jayachandran (1995), Effects of strain rate, temperature and thermomechanical coupling on the finite strain deformation of glassy polymers, *Mech. Mater.* 19, 193–212.

Bowden, P.B. (1973), The yield behavior of glassy polymers, in: *The Physics of Glassy Polymers*, ed. R.N. Haward, Applied Sci. Publ., Essex, p. 279.

Boyce, M.C., D.M. Parks and A.S. Argon (1988), Large inelastic deformation of glassy polymers, Part I: rate dependent constitutive model, *Mech. Mater.* 7, 15–33.

Haward, R.N. and G. Thackray (1968), The use of a mathematical model to describe isothermal stress–strain curves in glassy thermoplastics, *Proc. R. Soc. Lond. A* 302, 453–472.

Hutchinson, J.W. (1968), Singular behavior at the end of a tensile crack in a hardening material, *J. Mech. Phys. Solids* 16, 13–31.

Ishikawa, M. (1995), Stability of plastic deformation and toughness of polycarbonate blended with poly(acrylonitrile–butadiene–styrene) copolymer, *Polymer* 36, 2203–2210.

Jeong, H.-Y., X.-W. Li, A.F. Yee and J. Pan (1994), Slip lines in front of a round notch tip in a pressure-sensitive material, *Mech. Mater.* 19, 29–38.

Kramer, E.J. (1983), Microscopic and Molecular Fundamentals of Crazing, in: *Advances in Polymer Science* Vol. 52–53, Springer-Verlag Berlin, p. 1.

McMeeking, R.M. (1977), Finite deformation analysis of crack-tip opening in elastic–plastic materials and implications for fracture, *J. Mech. Phys. Solids* 25, 357–381.

Needleman, A. (1988), Material rate dependence and mesh sensitivity in localization problems, *Comp. Mech. Appl. Mech. Eng.* 67, 69–85.

Ni, B.Y., J.C.M. Li and V.K. Berry (1991), Plastic zone in front of a model I crack in acrylonitrile–butadiene–styrene polymers, *Polymer* 32, 2766–2770.

Parvin, M and J.G. Williams (1975), Ductile–brittle transitions in polycarbonate, *Int. J. Fract.* 11, 963–972.

Rice, J.R. (1968), A path independent integral and the approximate analysis of strain concentration by notches and cracks, *J. Appl. Mech.* 90, 379–386.

Rice, J.R. and G.E. Rosengren (1968), Plane strain deformation near a crack tip in a power law hardening material, *J. Mech. Phys. Solids* 16,1–12.

Rice, J.R. and M.A. Johnson (1970), The role of large crack tip geometry changes in plane strain fracture, in: *Inelastic Behavior of Solids*, eds. M.E. Kanninen, W.E. Adler, A.R. Rosenfield and R.I. Jaffee, McGraw-Hill, New York, p. 641.

Suo, Z., C.E. Shih and A.G. Varias, A theory for cleavage cracking in the presence of plastic flow, *Acta Metall. Mater.* 41, 1551–1557.

Williams, J.G. (1984), *Fracture Mechanics of Polymers*, Ellis Horwood, Chichester.

Wu, P.D. and E. Van der Giessen (1993), On improved network models for rubber elasticity and their applications to orientation hardening in glassy polymers, *J. Mech. Phys. Solids* 41, 427–456.

Wu, P.D. and E. Van der Giessen (1994), Analysis of shear band propagation in amorphous glassy polymers, *Int. J. Solids Struct.* 31, 1493–1517.

Wu, P.D. and E. Van der Giessen (1995), On neck propagation in amorphous glassy polymers under plane strain tension, *Int. J. Plast.* 11, 211–235.

Wu, P.D. and E. Van der Giessen (1996), Computational aspects of localized deformations in amorphous glassy polymers, *Eur. J. Mech. A*, 15, 799–823.

Yamamoto, T. and H. Furukawa (1995), Relationship between molecular structure and deformation–fracture mechanism of amorphous polymers: 2. Crazing stress, *Polymer* 36, 2393–2396.